Case Studies in Thermal Engineering 10 (2017) 343–356

Contents lists available at ScienceDirect

Case Studies in Thermal Engineering

journal homepage: www.elsevier.com/locate/csite

Conversion analysis of a cylindrical biomass particle with a DEM-CFD coupling approach

Mohammad Mohseni*, Bernhard Peters, Mehdi Baniasadi

University of Luxembourg, Faculty of Science, Technology and Communication, Campus Kirchberg, 6, rue Coudenhove-Kalergi, L-1359, Luxembourg

ARTICLE INFO

Keywords:
DEM-CFD
Heat/mass transfer
Biomass conversion
Porous particle

ABSTRACT

Biomass as a renewable energy source has attracted more attention nowadays due to ecological and economical benefits. The main objective of this work is studying the biomass conversion with employing a DEM-CFD coupling approach. In this model, the solid particulates are considered as discrete elements coupled via heat, mass and momentum transfer to the surrounding gas as continuous phase. That is, a comprehensive three-dimensional numerical model is developed and applied to investigate the complex phenomena taking place during biomass conversion in a reactor. In this case, the physical and chemical processes as heat-up, drying, pyrolysis, gasification and combustion are taken into account based on the relevant homogeneous and heterogeneous reactions. This platform predicts the motion of discrete particles based on the newton's equations of motion; and the thermodynamic state of each particle is extended according to the related algorithms. The thermodynamic state estimates the temperature and species distributions inside the particle due to external heat sources and chemical reactions. The reaction rates are described with Arrhenius model, and the reactions in the gas phase are modeled using Partially Stirred Reactor (PaSR) model with the standard $k-\epsilon$ turbulent model. The conductive and radiative heat transfer between particles as well as convective heat transfer between particles and gas phase are also observed. Due to layered behavior of biomass materials, the shape of particle is considered as cylindrical rather than spherical to predict more realistic results. In order to improve the numerical modeling of biomass conversion, a shrinkage model is also developed and validated with experimental data in literature.

1. Introduction

Conversion of biomass into usable energy sources represents a vital method of reducing fossil fuel dependence and greenhouse gas emissions. The low levels of impurities in biomass leads to lower SO_x and NO_x emission during conversion and thus reduced contribution to acid rain [1]. Fig. 1 shows four significant categories of yields produced via conversion of different waste and low-price resources of biomass. During biomass conversion, the physical and chemical processes as heat-up, drying, pyrolysis, gasification and combustion take place sequentially. These processes as shown in Fig. 2(a) are estimated according to homogeneous and heterogeneous reactions and discussed in the next section.

Biomass conversion depends on different parameters such as amount of produced volatile matter, yielded char, particle size, reactants partial pressure, reactor temperature and residence time. Many works are done concerning biomass conversion experimentally and numerically in various types of reactors. Tremel and Spliethoff [2] have studied volatile yield, char specific surface area, and char reactivity after pyrolysis experiments in a pressurized entrained flow fluidized bed. It is concluded that the devolatilization

* Corresponding author.
E-mail addresses: mohammad.mohseni@uni.lu, mohamad.mohseny@gmail.com (M. Mohseni).

http://dx.doi.org/10.1016/j.csite.2017.08.004
Received 28 May 2017; Received in revised form 16 August 2017; Accepted 25 August 2017
Available online 06 September 2017

Nomenclature

c_p	specific heat capacity at constant pressure, J/kg K
d_p	particle diameter, m
D	Diffusion coefficient, m^2/s
e	restitution coefficient, –
E	Young's modulus, N/m^2
$\mathbf{F}$	force, N
g	gravity, m/s^2
G	Shear modulus, N/m^2
h	enthalpy, J/kg
I	moment of inertia, J/kg
k	stiffness, N/m
K	permeability, m^2
L_v	latent heat of evaporation, J/kg
m	mass, kg
$\dot{m}$	mass flow rate, kg/s
p	pressure, Pa
Pr	Prandtl number, –
$\dot{q}$	heat flux, W/m^2
R	radius; radial coordinate, m
Re	Reynolds number, –
t	time, s
T	temperature, K
$\mathbf{T}$	torque, N m
v	velocity, m/s

Greek symbols

δ	differential operator, –
Δ	difference, –
α	heat transfer coefficient, W/m^2 K
β	mass transfer coefficient, m/s
ε	porosity, –
λ	thermal conductivity, W/m K
μ	dynamic viscosity, kg/m s
$\boldsymbol{\mu}$	friction coefficient, –
ν	kinematic viscosity, m^2/s
ρ	density, kg/m^3
τ	tortuosity, –
σ	Stefan-Boltzmann constant, W/m^2 K^4
ω	angular velocity, rad/s

Subscripts

D	drag
l	liquid
g	gas
i	initial
p	particle
s	solid
fp	fluid-particle interaction
ij	effective
n	normal
t	tangential

behavior of the solid fuels and the reactivity of the resulting char are important design parameters for entrained flow gasifiers. The experimental data indicate that the devolatilization rate is significantly faster than the char deactivation rate. In addition, Baruah in [3] categorizes the recent modeling works based on certain specific criteria such as type of gasifier, feedstock, modeling

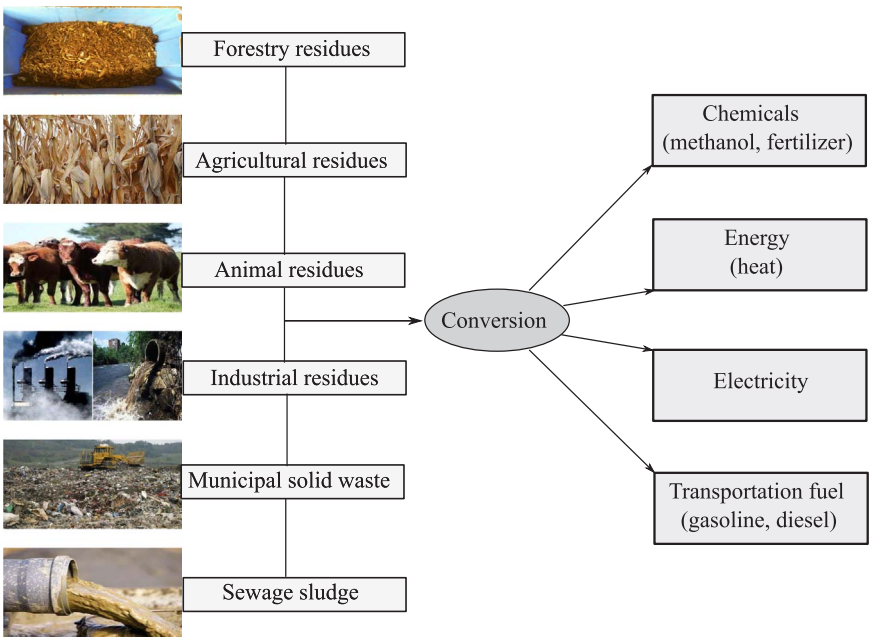

Fig. 1. Biomass resources (left) conversion to different products (right).

considerations and evaluated parameters. Apparently, feed stock flow rate, gasifying agent flow rate, equivalence ratio, reactor pressure and temperature are some of the important operating parameters which influence the conversion process. Change in a parameter has considerable effect on the flue-gas composition and hence on the performance of the reactor.

Furthermore, Babu in [4] predicts the composition and temperature profiles across the length of the reduction zone using a steady state equilibrium model. It is shown that the char reactivity factor is the key parameter in modeling the downdraft gasifier, and it directly represents the reactivity of the char in the reduction zone. Melgar et al. [5] has proposed a thermochemical equilibrium model for downdraft gasifiers to predict the final produced gas composition and its main characteristics such as heating value and engine fuel quality for a biomass with a defined ultimate composition and moisture content. The reaction temperature is considered to be the driving parameter of the whole conversion process and calculated considering thermal equilibrium. Through the energy equation, the reaction temperature corresponding to a certain fuel/air ratio and moisture content is obtained, and thereby the reaction temperature is estimated.

Besides, Gao and Li in [6] simulated the behavior of a fixed bed biomass in a gasifying reactor to study the effect of heating rate and fixed temperature of the pyrolysis zone on the flue-gas composition. It was observed that for a continuous heating rate of the pyrolysis zone, the concentrations of H_2 and CO increased while those of N_2 and CO_2 decreased with increasing reaction temperature. The CH_4 content is increased during the reaction time, while it is decreased at the end of the reaction. Similar observations were made for H_2O fraction. For a constant pyrolysis temperature, CO_2 decreased and CH_4, H_2, CO and H_2O increased with reaction time. In both modes, the trends of temperature profile and species concentrations were found to be very different. Thus, it is observed that modeling the pyrolysis and reduction zones together, the temperature profile of the pyrolysis zone has significant effect on the gas composition in the reduction zone [3]. Also Azzone et al. in [7] developed an equilibrium model for the simulation of thermochemical gasification applied to agricultural residues. The model behavior was analyzed by varying process parameters (pressure, temperature), biomass humidity and oxidant agent composition. It is proved that by increasing the pressure in the gasifier, the methane fraction increased. This was due to the fact that the equilibrium constant is inversely proportional to the process pressure.

In multiphase flows to investigate the effect of solid material in the fluid flow, the porous media concept is employed. Porous medium by definition is a material involving a solid matrix with an interconnected void so that the solid matrix could be either rigid (the usual situation) or it sustains small deformation. The interconnectedness of the void spaces allow the fluid to flow through the material in which by a single fluid (gas or liquid) is called single-phase flow or with both liquid and gas sharing the void space is named two-phase flow. But the shape and size of pores are irregular in the porous medium [8]. In porous media the continuum mechanics deals with transition from the molecular scale to the micro-scale (pore-scale) to resolve the flow in pore spaces. This is done with replacing the molecular properties by averaged properties over a large number of molecules. That is, instead of each molecule, the overall fluid flow is considered with averaged fluid properties such as density and viscosity. In addition, in the fluid mechanics a continuum needs to be considered at the macro-scale. To fulfill the transition from micro-scale to macro-scale, the micro-

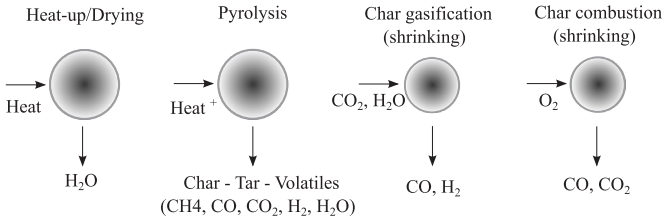

(a) Main steps of conversion process

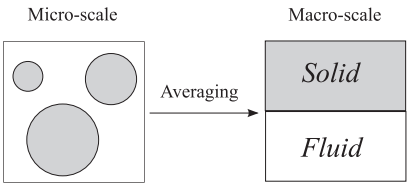

(b) Volume averaging from micro-scale to macro-scale in a typical 2D cell

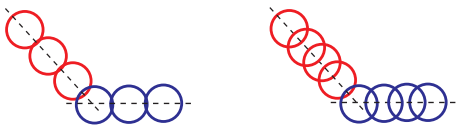

(c) Sub-spherical particles representing cylindrical shape; left: simple, right: packed

Fig. 2. Conversion process, volume averaging and sub-spherical model.

scale is expressed as a grid cell including porous structure. In this case, the micro-scale properties are averaged over a representative elementary volume (REV) to obtain a macro-scale description of the system so that the effective parameters are porosity and intrinsic permeability. Fig. 2(b) shows the volume averaging transition from micro-scale to macro-scale as well as porous structure thereby the DEM-CFD approach in this study is based on.

Since the biomass materials have layered behavior similar to an insulator, the suitable model for biomass is either slab or cylinder where the latter is applied in this study. Recently, the studies on modeling non-spherical particles are increased significantly. Lu et al. in [9] reviews the DEM modeling of non-spherical particle systems which remarks the advances in shape representation algorithms and efficient detection of contacts. Also Zhong et al. [10] reviews extensively the theoretical developments and applications of DEM modeling in non-spherical particle systems. Dziugys and Peters in [11] introduce a new algorithm to calculate analytically the overlap of two-dimensional ellipses based on the general equation of superquadratics.

In this work, the cylindrical particle with non-spherical shape is replaced by a sub-spherical configuration. Fig. 2(c) shows a cylindrical particle represented by sub-spheres which approximately fills the original particle shape. To improve the approximation, it is feasible to increase the number of sub-spheres where the packed configuration (see Fig. 2(c) right) with 4-sphere is considered in this study. In this approach, which is originally proposed by Nolan et al. [12], it is assumed that the sub-spheres could have different sizes, but the whole shape remains a rigid body with constant distance between sub-spheres. The advantage is the contact between original shapes is considered as contacts between their sub-shapes meaning the contact detection remains the same as spherical contacts for simplicity. It is noted that the total force and torque acting on a non-spherical particle is calculated based on total forces and torques of the sub-shapes, but at the center of gravity of the original shape. Although, this method specifies the original shape

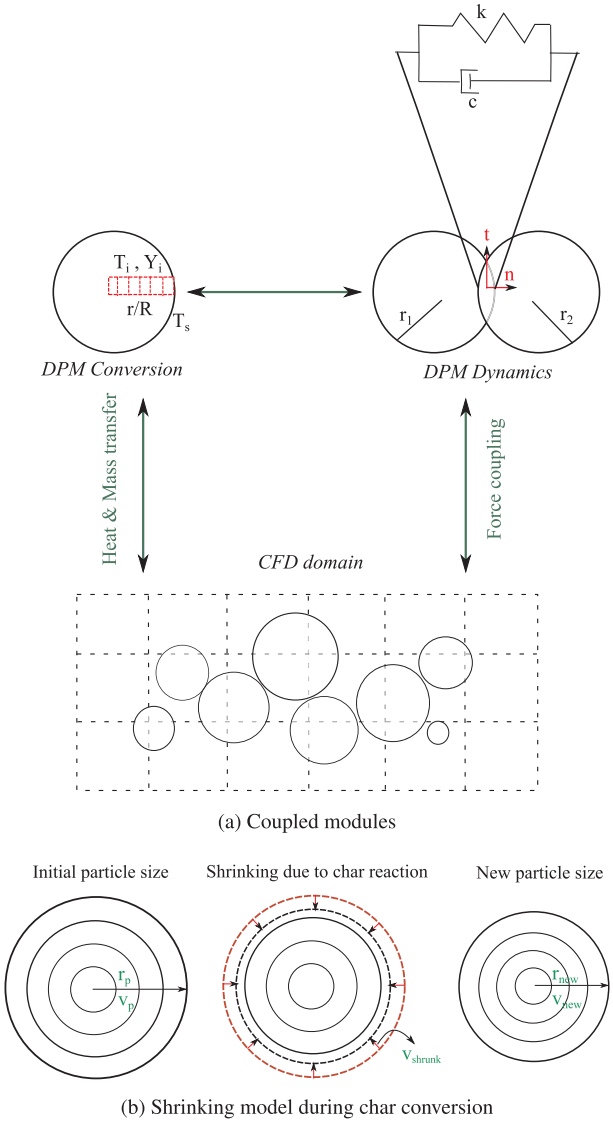

Fig. 3. Schematic of DEM-CFD approach.

with no absolute precision, but with an acceptable approximation for applications [13].

The aim of this study is applying a DEM-CFD coupling module to predict the conversion of biomass in a reactor. In this approach; which considers the particles as discrete elements and the gas flow as continuous phase; the dynamics behavior of granular flow through the gas phase, as well as the physical and chemical processes are considered simultaneously. In this case, the conversion behavior of a single particle with cylindrical shape is investigated and validated with experimental data in literature. Due to remarkable influence of shrinkage during biomass conversion, a shrinking model is also developed and evaluated.

2. Mathematical modeling

Since experimental work is highly expensive and time-consuming, the numerical modeling is an alternative tool to find out the complex phenomena inside the industrial reactors. In this work, a DEM-CFD coupling approach is employed to model the physical and chemical phenomena taking place inside a reactor. This advanced numerical method in multi-physics and multi-scale systems models the dynamics of particulates based on the classical discrete element method originally proposed by Cundall and Strack [14]. In addition, the thermodynamic state of each particle is considered according to the related algorithms to estimate the temperature and species distribution through the particle. To simulate the continuous fluid phase, OpenFOAM source code as a computational fluid dynamics (CFD) tool is coupled to the discrete phase. This makes a robust and reliable tool to deal with industrial applications involving heat-up, drying, pyrolysis, combustion and gasification processes. Fig. 3(a) describes the DEM-CFD coupling modules.

The translational and rotational motion of each particle are defined according to the Newton's second law so that the explicit finite difference scheme is employed to solve the motion equations. Table 1 represents the equations of motion of particle related to interactions between particle-particle and particle-gas phase. Where i denotes each particle; m_i and I_i are mass and moment of inertia; $\vec{\mathbf{v}}_{p,i}$ and $\vec{\omega}_i$ are particle velocity and angular velocity; $\vec{\mathbf{F}}_{c,i}$, $\vec{\mathbf{F}}_{fp,i}$, $m_i\vec{\mathbf{g}}$ and $\vec{\mathbf{T}}_i$ are contact force between particle-particle and particle-wall, drag force acting on particles by gas flow, gravitational force and torque acting on particles by tangential component of impact force. The key point in contact detection is evaluating the overlap between a pair of particles where non-linear Hertz-Mindlin model is employed to estimate interaction force. $\vec{\mathbf{F}}_{fp}$ is the interface term referred to force coupling between DEM-CFD modules. It implies the drag force impact on particles where c and i are cell and particle index; N_c and V_c are number of cells and cell volume; and $\mathbf{f}_{d,i}$ denotes the drag force applied on each particle in the cell which is correlated to the particle and fluid velocities [15].

In order to predict the interactive drag force between the particles and surrounding fluid phase, many studies have concentrated to calculate the interfacial momentum exchange or the drag correlation B_i with developing different methods. The Gidaspow model is

Table 1
Particle motion governing equations.

Particle translational motion equation:

$$m_i\frac{d\vec{\mathbf{v}}_{p,i}}{dt} = \vec{\mathbf{F}}_{c,i} + \vec{\mathbf{F}}_{fp,i} + m_i\vec{\mathbf{g}} \tag{1}$$

Particle rotational motion equation:

$$I_i\frac{d\vec{\omega}_i}{dt} = \vec{\mathbf{T}}_i \tag{2}$$

Solid- fluid interaction force equation:

$$\vec{\mathbf{F}}_{fp} = \sum_{i=1}^{N_c}\frac{\varepsilon_f\mathbf{f}_{d,i}}{V_c} \tag{3}$$

$$\mathbf{f}_{d,i} = B_i(\vec{\mathbf{v}}_{fi} - \vec{\mathbf{v}}_{pi}) \tag{4}$$

$$B_i = \begin{cases} 150\mu_f\dfrac{(1-\varepsilon_f)^2}{\varepsilon_f d_{pi}^2} + 1.75(1-\varepsilon_f)\dfrac{\rho_g}{d_{pi}}|\vec{\mathbf{v}}_f - \vec{\mathbf{v}}_{pi}|, & \text{for } \varepsilon_f \le 0.8 \text{ (Ergun)} \\ \dfrac{3}{4}C_{Di}\rho_f\varepsilon_f^{-2.7}\dfrac{\varepsilon_f(1-\varepsilon_f)}{d_{pi}}|\vec{\mathbf{v}}_f - \vec{\mathbf{v}}_{pi}|, & \text{for } \varepsilon_f > 0.8 \text{ (Wen} - \text{Yu)} \end{cases} \tag{5}$$

$$C_{Di} = \begin{cases} \dfrac{24}{\varepsilon_f Re_{pi}}(1 + 0.15(\varepsilon_f Re_{pi})^{0.687}), & \text{for } Re_{pi} < 1000 \\ 0.44 & \text{for } Re_{pi} \ge 1000 \end{cases} \tag{6}$$

$$Re_{pi} = \frac{d_{pi}\rho_f\varepsilon_f}{\mu_f}|\vec{\mathbf{v}}_f - \vec{\mathbf{v}}_{pi}| \tag{7}$$

reported as the best fitted approach in [16] via investigating through various methods compared to experimental data. The reason that Gidaspow model [17] has employed successfully in many works is it includes both high and low porosity regions due to the fact that the void fraction has great influence on the drag force calculation. The Gidaspow drag model is a combination of Ergun equation and Wen-Yu model. The Ergun equation is related to the dense beds and considers the drag force as pressure drop among the porous media. On the other hand, the Wen-Yu model observes the high porosity regions when the viscous forces are dominant. The first part of Ergun equation describes low Reynolds number, while the second part explains high Reynolds number flow.

In this DEM-CFD coupling approach, the processes inside each particle is described by one-dimensional and transient conservation equations in radius direction shown in Fig. 3(a). This is accurate enough based on the study by Man and Byeong in [18]. With summing individual particle processes, the total process is established for the packed bed of particles. The arrangement of particles within the surrounding gas is expressed as void space. In this case, the flow through the void space of the packed bed is modeled as the flow through a porous medium with considering the interaction between the solid-gas phase by heat, mass and momentum transfer [19].

For compressible flows within porous media described in Fig. 2(b), the conservation equations of mass, momentum, energy and species transport are presented in Table 2. In continuity equation, the mass source (S_{mass}) is caused by mass transfer through the particles and the variable r is defined to distinguish between different domains as an infinite plate ($n = 0$), an infinite cylinder ($n = 1$) and a sphere ($n = 2$). In momentum equation, the Darcy law in Hager [20] is employed to implement gas species transport through pore spaces of a particle. Regarding energy equation, the LHS terms represent the accumulation of enthalpy. The first RHS term describes the contribution of convective flow to the accumulation of enthalpy and the last RHS term represents the enthalpy from formation/consumption rate of i specie ($i = 1...k$). Also the conservation equation of species describes the time and spatially varying concentration of specie (i) where $Y_{i,g}$ and $\dot{w}_{i,g}$ are gas specie (i) concentration and it's rate as a source term. Due to averaging process

Table 2
Discrete elements governing equations.

Continuity equation

$$\frac{\partial}{\partial t}(\varepsilon_p\langle\rho_f\rangle) + \frac{1}{r^n}\frac{\delta(r^n\varepsilon_p\langle\rho_f\rangle\langle\vec{\mathbf{v}}_f\rangle)}{\delta r} = S_{mass} \tag{8}$$

Momentum equation

$$\frac{\varepsilon_p\mu_f}{K^*}\langle\vec{\mathbf{v}}_f\rangle = -\frac{\delta(\varepsilon_p p)}{\delta r} \tag{9}$$

Energy equation

$$\frac{\delta\langle\rho c_p T\rangle}{\delta t} = \frac{1}{r^n}\frac{\delta}{\delta r}\left(r^n\lambda_{eff}\frac{\delta\langle T\rangle}{\delta r}\right) + \sum_{i=1}^{k}\dot{w}_k H_k \tag{10}$$

Species equation

$$\frac{\delta Y_{i,f}}{\delta t} + \frac{1}{r^n}\frac{\delta(r^n Y_{i,f}\langle\vec{\mathbf{v}}_f\rangle)}{\delta r} = \frac{1}{r^n}\frac{\delta}{\delta r}\left(r^n D_{i,eff}\frac{\delta\langle Y_{i,f}\rangle}{\delta r}\right) + \dot{w}_{i,f} \tag{11}$$

Boundary conditions

$$-\lambda_{eff}\frac{\delta\langle T\rangle}{\delta r}\bigg|_{r=0} = 0 \tag{12}$$

$$-\lambda_{eff}\frac{\delta\langle T\rangle}{\delta r}\bigg|_{r=R} = \alpha(T_R - T_\infty) + \dot{q}_{rad} + \dot{q}_{cond} \tag{13}$$

$$-D_{i,eff}\frac{\delta\langle c_i\rangle}{\delta r}\bigg|_{r=R} = \beta_i(c_{i,R} - c_{i,\infty}) \tag{14}$$

$$\alpha = \frac{\dot{m}_g c_{p,g}}{\exp(\dot{m}_g c_{p,g}/\alpha_0) - 1}; \quad \beta = \frac{\dot{m}_g/\rho_g}{\exp(\dot{m}_g/\rho_g\beta_0) - 1} \tag{15}$$

$$\lambda_{eff} = \varepsilon_p\lambda_g + \eta\lambda_{solid} + (1-\eta)\lambda_{char} + \lambda_{rad}; \quad \lambda_{rad} = \frac{4\varepsilon_p}{1-\varepsilon_p}\sigma T^3 \tag{16}$$

$$D_{i,eff} = D_i\frac{\varepsilon_p}{\tau.} \tag{17}$$

and influence of tortuosity (τ) on the diffusion, an effective diffusion coefficient is defined so that the molecular diffusion coefficient (D_i) is taken from the equivalent ones of appropriate species in nitrogen [21–23].

Besides, the specified boundary conditions (also described in Peters [24]) complete resolving the governing equations. Where T_∞, c_i, α and β denote ambient gas temperature, concentration of specie (i), heat and mass transfer coefficients. The mass transfer coefficients employed are valid for vanishing convective fluxes. These convective fluxes e.g. volatiles and vapor out of and into the particle are important transfer coefficients that have to be corrected according to the Stefan correction [25] defined with α_0 and β_0. RHS of effective thermal conductivity λ_{eff} represents the participation of conduction heat transfer in gas, solid, char and by radiation [24].

In this approach, the governing equations of fluid flow are described by implementing porous media concept into conservation equations proposed in Faghri and Zhang [26]. In order to discretize the equations, the finite volume method is used and all variables are stored on the centers of structured cells. Table 3 presents locally averaged conservation equations of mass, momentum, energy and species transport including the required boundary conditions for the fluid phase. The detail of implementation is referred to [26]. In order to explain the interaction between solid-fluid phases; the interfaces of mass, momentum, energy and species transport are described via S_{mass}, $\vec{\mathbf{F}}_{fp}$, $\sum_{i=1}^{k} \dot{w}_k H_k$ and $\dot{w}_{i,f}$ terms in the conservation equations.

In this part, the physical and chemical processes taking place during biomass conversion are discussed. To explain drying, the rate of water evaporation needs to be estimated. In this case, there are three approaches as heat sink, first order kinetic evaporation rate and equilibrium model. In this work the heat sink model is used so that the available heat above the saturation temperature T_{sat} is consumed for evaporation of particle moisture content. Eq. (25) calculates the rate of water evaporation which is defined as a source term in species equation. The prediction of saturation temperature (T_{sat}) is based on the particle operating pressure (P) with an empirical correlation function shown in Eq. (26).

$$\dot{w}_{H_2O} = \begin{cases} \dfrac{\rho_g C_p (T - T_{sat})}{H_{sat}\,\delta t}, & \text{for } T \geq T_{sat} \\ 0 & \text{for } T < T_{sat} \end{cases} \tag{25}$$

$$T_{sat} = 342.473 + 36.4857(P/10^5) - 6.5274(P/10^5)^2 + 0.5056(P/10^5)^3 \tag{26}$$

After drying process, pyrolysis is a crucial pre-step reaction prior to combustion and gasification. After depletion of water content, the temperature of particle raises with increasing heat. In this moment, the particle commences to decompose thermally to char, tar and volatiles defined as three reactions shown bellow. By definition, pyrolysis is thermochemical decomposition of biomass into useful products where large complex hydrocarbon molecules of biomass are broken down into smaller and simpler molecules. The

Table 3
Continuous phase governing equations.

Continuity equation

$$\frac{\partial}{\partial t}(\varepsilon_f \langle \rho_f \rangle) + \nabla . (\varepsilon_f \langle \rho_f \rangle \langle \vec{\mathbf{v}}_f \rangle) = S_{mass} \tag{18}$$

Momentum equation

$$\frac{\partial}{\partial t}(\varepsilon_f \langle \rho_f \rangle \langle \vec{\mathbf{v}}_f \rangle) + \nabla . (\varepsilon_f \langle \rho_f \rangle \langle \overrightarrow{\mathbf{v}_f \mathbf{v}_f} \rangle) = -\nabla p + \nabla . \left(\varepsilon_f \langle \overrightarrow{\tau' _f} \rangle \right) - \vec{\mathbf{F}}_{fp} \tag{19}$$

Energy equation

$$\frac{\partial}{\partial t}(\varepsilon_f \langle \rho_f \rangle \langle h_f \rangle) + \nabla . (\varepsilon_f \langle \rho_f \rangle \langle \vec{\mathbf{v}}_f h_f \rangle) = \frac{\partial \langle p_f \rangle}{\partial t} + \varepsilon_f \langle \vec{\mathbf{v}}_f \rangle . \nabla \langle p_f \rangle + \sum_{i=1}^{k} \dot{w}_k H_k \tag{20}$$

Species equation

$$\frac{\partial}{\partial t}(\varepsilon_f \langle \rho_{f,i} \rangle) + \nabla . (\varepsilon_f \langle \rho_{f,i} \rangle \langle \vec{\mathbf{v}}_f \rangle) = \dot{w}_{i,f} \tag{21}$$

Boundary conditions

$$-K \frac{\partial \langle T \rangle}{\partial r}\bigg|_{wall} = 0 \tag{22}$$

$$\langle \vec{\mathbf{v}}_f \rangle|_{in} = (u_{in}, 0, 0) \tag{23}$$

$$\langle \vec{\mathbf{v}}_f \rangle|_{wall} = (0, 0, 0) \tag{24}$$

quality of products depends on several factors such as the reactor design, biomass characteristics, pyrolysis temperature, residence time and heating rate. Table 4 introduces the pyrolysis reactions which take place via *heterogeneous* reactions in the solid phase. Where α_i is the mass fraction of volatile species taken from Blasi [27] listed in Table 6.

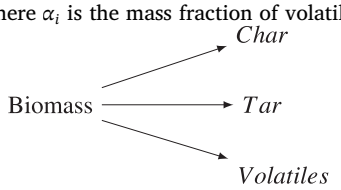

The volatile matters released from devolatilization react with existing oxygen in the system and produce required heat for the endothermic reactions. The *homogeneous* reactions in Table 4 are employed in this work for modeling combustion of volatiles. Moreover, the released char is also combusted and gasified according to the *heterogeneous* reactions shown in Table 4. And the reaction rates are presented in Table 5 so that the reaction rate constant is calculated based on Arrhenius form ($K_i = A_i exp(E_i/RT)$). To describe the turbulence/chemistry interaction, the Partially Stirred Reactor model (PaSR) in combination with $k-\epsilon$ turbulence model is applied. That is, in addition to considering heat, mass and momentum transfer in the system, the kinetics of reactions (in Table 7) is involved to evaluate produced char, tar and volatile matters at any operating condition. It is assumed that involved gases in the processes are ideal gas, and nitrogen as an inert has no contribution in the chemical reactions. Regarding the char combustion reaction (No. 9 in Table 4), the value of the partition coefficient (γ) depends on the temperature inside the system and lies between 1 and 2. The expression below is used in this study which is based on [28–30] and T_p is the surface temperature of char at any operating time.

$$\gamma = \frac{2(1 + 4.3\exp(-3390/T_p)}{2 + 4.3exp(-3390/T_p)} \tag{27}$$

Under similar conditions, the combustion reactions are faster than gasification reactions. During gasification, the temperature of solid char is nearly the same as bed temperature due to the simultaneous exothermic and endothermic reactions on it. In combustion, char temperature can be much hotter than the bed temperature [31]. The rate of char combustion and gasification are calculated according to Evan and Emmons [32], which are based on the partial pressure of oxidizing and gasifying agent within the particle.

In particle scale modeling it is assumed that particles are isotropic and the properties change along the radius where the distribution of temperature and species within the particle are described by a system of one-dimensional and transient conservation equations. During conversion since the solid particle lose its mass; the shrinkage is considered for pyrolysis, combustion and gasification processes except drying due to negligible volume change [30]. Basically, the shrinking improves heat and mass transfer due to surface reduction and smaller dimension [36]. In the shrinking model developed in this work, it is assumed that the char formation during pyrolysis and char consumption by gasification and combustion is in the outermost cell (V_{cell}) of the particle. In fact, the porosity and radius of the particle vary so that char reaction rate ($\dot{w}_{char}$) in the boundary cell of the particle influences the shrinking volume. The shrunk volume (V_{shrunk}) and reduced size of particle (r_{new}) are defined as:

$$V_{shrunk} = \frac{\dot{w}_{char} * V_{cell}}{\rho_p} \tag{28}$$

$$r_{new} = \sqrt{\frac{V_p - V_{shrunk}}{\pi l}} \tag{29}$$

Table 4
Stoichiometric equations of pyrolysis, combustion and gasification for modeling thermal conversion of wood.

Reaction no.	*Reaction definition*
Pyrolysis reactions:	
1	$Wood \rightarrow Char$
2	$Wood \rightarrow Tar$
3	$Wood \rightarrow \alpha_1 CH_4 + \alpha_2 CO + \alpha_3 CO_2 + \alpha_4 H_2 + \alpha_5 H_2O$
Homogeneous reactions:	
4 – *CO combustion*	$2CO + O_2 \rightarrow 2CO_2$
5 – *CH_4 combustion*	$CH_4 + 2O2 \rightarrow CO_2 + 2H_2O$
6 – *H_2 combustion*	$2H_2 + O_2 \rightarrow 2H_2O$
7 – *Tar combustion*	$Tar + 2.9O_2 \rightarrow 6CO + 3.1H_2$
Heterogeneous reactions:	
8 – Char combustion	$\gamma C(s) + O_2 \rightarrow 2(\gamma - 1)CO + (2 - \gamma)CO_2$
9 – Steam gasification	$C(s) + H_2O \rightarrow CO + H_2$
10 – Boudouard	$C(s) + CO2 \rightarrow 2CO$

Table 5
Reaction rate estimation.

Reaction no.	$\dot{w}_i$=	*Ref.*
1	$\frac{\delta\rho_{wood}}{\delta t} = K_1\rho_{wood}$	
2	$\frac{\delta\rho_{wood}}{\delta t} = K_2\rho_{wood}$	
3	$\frac{\delta\rho_{wood}}{\delta t} = K_3\rho_{wood}$	
4	$\frac{\delta[CO]}{\delta t} = K_5[CO][O_2]^{0.25}[H_2O]^{0.5}$	
5	$\frac{\delta[CH_4]}{\delta t} = K_6[CH_4]^{0.7}[O_2]^{0.8}$	
6	$\frac{\delta[H_2]}{\delta t} = K_7[H_2][O_2]$	
7	$\frac{\delta[tar]}{\delta t} = K_8T[tar]^{0.5}[O_2]$	
8	$\frac{\delta\rho_{O_2}}{\delta t} = K_9P_{O_2}S_{a,char}$	[32]
9	$\frac{\delta\rho_{CO_2}}{\delta t} = K_{10}P_{CO_2}S_{a,char}$	[32]
10	$\frac{\delta\rho_{H_2O}}{\delta t} = K_{11}P_{H_2O}S_{a,char}$	[32]

Table 6
Volatiles mass fraction of the pyrolysis reaction No. 3.

	CH_4	CO	CO_2	H_2	H_2O
α_i [33]	0.031	0.156	0.271	0.021	0.521

Table 7
Reactions kinetic data to calculate K_i.

Reac no.	*A*	*E* (kJ/kg)	ΔH (kJ/kg)	*Ref.*
1	3.27×10^6	111.7	− 418	[33]
2	1.08×10^{10}	148	− 418	[33]
3	4.38×10^9	152.7	− 418	[33]
4	2.24×10^{12}	167.36	10,110	[34]
5	11.58×10^{13}	202.5	50,187	[34]
6	2.19×10^9	109.2	120,900	[34]
7	9.2×10^6	80.2	17,473	[35]
8	2.54×10^{-3}	74.8	*Change with* γ	[32]
9	1.81×10^{-2}	130	− 14,370	[32]
10	1.81×10^{-2}	130	− 10,940	[32]

The reactions taking place inside the particle increase the porosity of particle instead. The particle size reduction due to shrinking is shown in Fig. 3(b) where the circles inside the particle show the number of arbitrary cells defined in the particle modeling. After reduction, the particle with new size is generated with the same number of cells for numerical stability. The shrinking model is applicable for different shapes such as slab, sphere and cylinder. In this model, it is assumed that the particle shrinks uniformly in radial direction and the original shape of the particle remains unchanged. This means for the cylindrical shape applied in this study, the length of the cylinder and accordingly the number of sub-spheres remain unchanged.

3. Case definition

Fig. 4 shows the simulation case applied in this study which is a cylindrical chamber based on the work by Wiese et al. [28]. In order to evaluate the conversion of biomass fuel, a single cylindrical beechwood particle is simulated at two different wall reactor temperature (700, 800 °C). Table 8 presents the proximate and ultimate analysis of the biomass fuel. And the particle and gas properties are listed in Tables 9, 10. There exist two inlets and one outlet at the top of reactor. The primary inlet is injected from the bottom and passes the underneath grate and particle. In the simulation case, there is a gap (20 mm) between the primary inlet and particle to consider the developed flow reaching the particle. The secondary inlet is located at 88 mm above the grate so that air flows through a distribution chamber surrounding the reactor and enters via circular inlet. In this case study, heat is significantly provided by the hot wall with temperature of 700 − 800 °C. That is the radiation from the reactor wall to the particle surface is considered. As stated, to describe the heat and mass transfer within the particle, it is spatially divided into multiple radial cells where the resolution of particle discretization is determined by the number of cells. In this work since the radius of cylindrical particle is 6 mm, the number

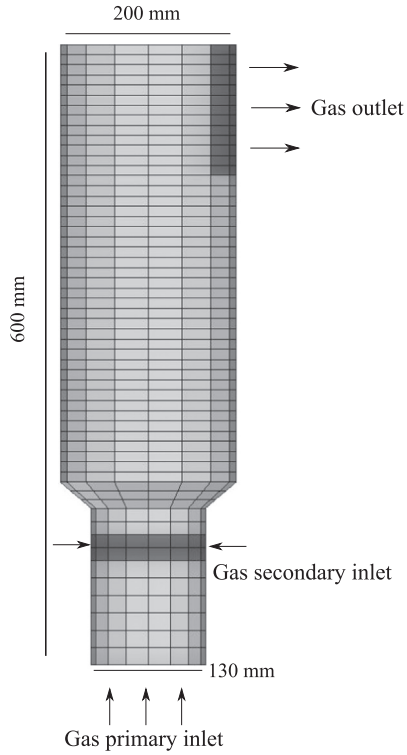

Fig. 4. Gas CFD domain with primary and secondary inlets and upper outlet.

Table 8
Initial and final fuel composition.

Proximate Analysis – As-Received basis [28]	
Moiture (wt%)	6.82
Fixed carbon (wt%)	14.39
Ash (wt%)	0.19
Volatiles (wt%)	78.6
HHV (MJ/kg)	17.38
Ultimate Analysis – dry and ash free(daf) basis [28]	
C (wt%)	51.7
H (wt%)	6.13
N (wt%)	0.23
O (wt%)	41.9
S (wt%)	0.04

of cells in radius direction is 6 as well. Besides, the convective heat transfer between the solid and gas phase is calculated by Nusselt correlation of Wakao [37] and the relative convective mass transfer is analogical to the convective heat transfer with Sherwood number instead.

4. Result and discussion

To investigate the biomass conversion with shrinkage, a single pellet particle is investigated based on [28]. Two conditions are performed for each wall temperature (700, 800 °C) considering with and without the shrinking model. Fig. 5(a) shows the prediction of mass loss tendency for the cylindrical particle during conversion compared to the experiment. As can be seen, the mass loss trend could be divided to four steps. For the wall temperature of 700 °C, since the particle is initiated at 25 °C, the first step is heat-up. This process is very fast due to high radiative heat transfer by wall. Then drying starts after reaching the particle temperature to saturation status. In this period which lasts 35 s, the temperature of particle remains constant and there is an equilibrium between water liquid and vapor inside the particle. Subsequently, the pyrolysis commences with converting beechwood to char, tar and volatile matters. In this moment, the particle starts getting shrunk and more porous. Afterwards, with leaving the volatiles from the particle, char gasification takes place due to reaction with steam and carbon dioxide released by combustion of volatiles. Moreover, the oxygen can enter the pore space of the particle where the combustion of char starts. It is obvious that all processes take place in a faster rate for

Table 9
Properties of the beechwood cylindrical particle.

diameter	d_p	6 [mm]
length	l_p	16.5 [mm]
density	ρ_p	1220 [kg/m^3]
initial temperature	T_0	25 [°C]
initial water content	X_0	1.1 [g water/g dry solid]
Young's modulus	Y	0.1 [GPa]
Poisson's ratio	ν	0.29
restitution coefficient	e	0.98
friction coefficient	μ_f	0.3
specific heat	c_p	1.5 + 0.001T [kJ/kg]
conductivity	λ	0.47 [W/m K]
permeability	K	0.02
pore diameter	–	50 [μm]
particle porosity	ε_p	0.64
DEM timestep	Δt_{solid}	10^{-5} [s]
CFD timestep	Δt_{fluid}	10^{-5} [s]

Table 10
Properties of the inlet air flow.

pressure	P	1 [bar]
temperature	T_g	25 [°C]
density	ρ_g (25 °C)	1.1707 [kg/m^3]
primary-air volume flow rate	$\dot{v}_{g,1}$	0.0023 [m^3/s]
secondary-air volume flow rate	$\dot{v}_{g,2}$	0.0046 [m^3/s]

the wall temperature of 800 °C rather than 700 °C. That means the conversion ends up faster due to higher heat transfer rate. As expected, the shrinking model improves the predictions of conversion according to experiments for both wall temperature.

In addition, Fig. 5(b) shows the effect of shrinking model based on the particle porosity and radius change for wall temperature of 700 °C. When the pyrolysis commences after 35 s, the particle radius remains unchanged for the model without shrinking, while the particle porosity tends to increase due to ongoing mass loss. In contrast, the prediction including the shrinking model leads to radius reduction because of shrinkage effect. In this case, there are two distinct rates starting from 40 s and 80 s which denote the onset of pyrolysis and gasification/combustion periods, respectively.

Besides, Fig. 5(c) represents the behavior of particle core temperature and it's rate during conversion of beechwood pellet at T_{wall} = 700 °C. At the beginning, since the particle is initiated at ambient temperature (25 °C) and because of high wall temperature (leading to high radiation heat transfer), the heating rate is intense. This leads to increase the temperature of particle rapidly to reach the saturation status (heat-up process). In this moment, drying starts and the particle temperature remains constant at around 100 °C in pressure 1 bar. This is shown as steady rate of temperature change with zero value between 10 and 35 s. At the end of drying, the particle temperature rises promptly due to high wall temperature and high heating rate where the pyrolysis starts. During devolatilization the heating rate decreases and it remains almost constant specially between 60 and 70 s. In this moment since the pyrolysis is terminated, the temperature of particle rises and accordingly the heating rate has another jump. This is due to the onset of char gasification and combustion explained in Fig. 6(b) as well.

Moreover, Fig. 6(a) illustrates the mass fraction of volatile yields during conversion of cylindrical beechwood particle at T_{wall} = 700 °C. Due to high heating rate at the beginning, the particle temperature reaches the saturation status rapidly so that drying starts at t = 6 s. During drying process until around 35 s, the only released gas is water vapor. That comes from evaporation of water liquid inside the particle due to equilibrium between water vapor and liquid. After drying and then increasing the particle temperature, the pyrolysis begins with delivering the volatiles CO_2, CO, CH_4, H_2, H_2O. This stage carries on until end of devolatilization process. The gas compositions released by the solid fuel are mixed with oxygen and combusted above the particle in the reactor. Consequently, these exothermic reactions generate required energy at the end of pyrolysis leading to minor gasification and combustion of char product.

Fig. 6(b) demonstrates the performance of solid material during pellet conversion at T_{wall} = 700 °C. At the beginning, the solid material is purely beechwood which means drying is taking place. When it terminates, the temperature of particle increases and then the pellet starts to decompose. Since beechwood is decomposed to volatiles faster than to char, the gas compositions are first released (at 35 s in Fig. 6(a)), while char is formed after t = 40 s. During pellet consumption, the char is formed until 80 s and afterwards it starts to convert partially via char gasification with carbon dioxide and char combustion with oxygen.

At the end, Fig. 6(c) shows the performance of liquid materials during beechwood conversion at T_{wall} = 700 °C. As can be seen, after heating-up and when drying starts, the water content evaporates until 35 s where all water liquid is vaporized. Then the pyrolysis commences thereby the tar liquid begins to form. Due to liquid mass transport, the yielded tar leaves the particle until 80 s.

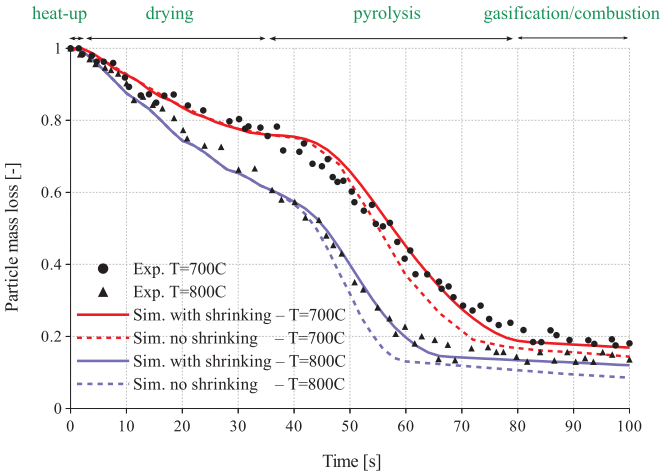

(a) Mass loss at $T_{wall} = 700,\ 800°C$

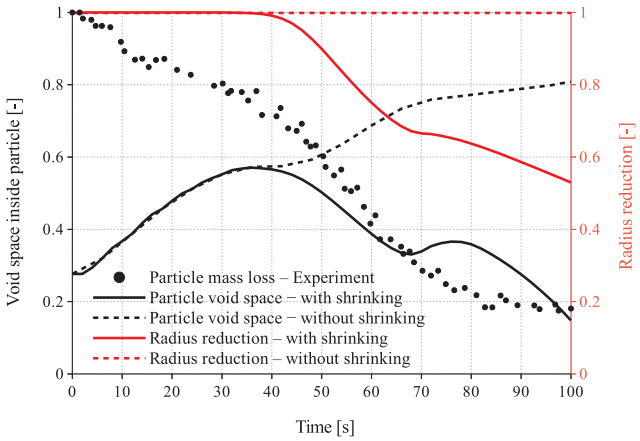

(b) Particle porosity and radius reduction at $T_{wall} = 700\ °C$

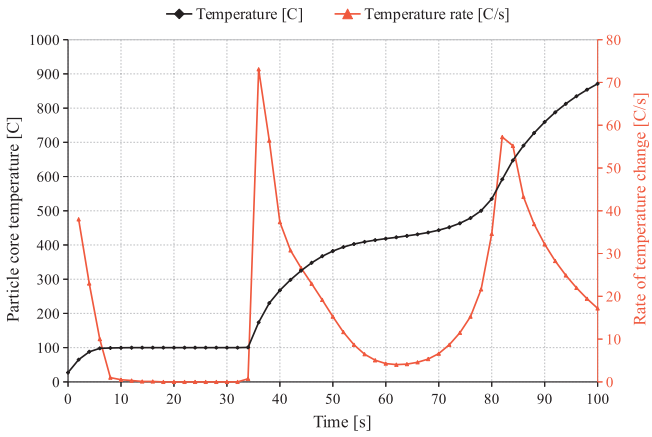

(c) Particle temperature and temperature change rate at $T_{wall} = 700\ °C$

Fig. 5. Simulation and experimental results of cylindrical particle conversion.

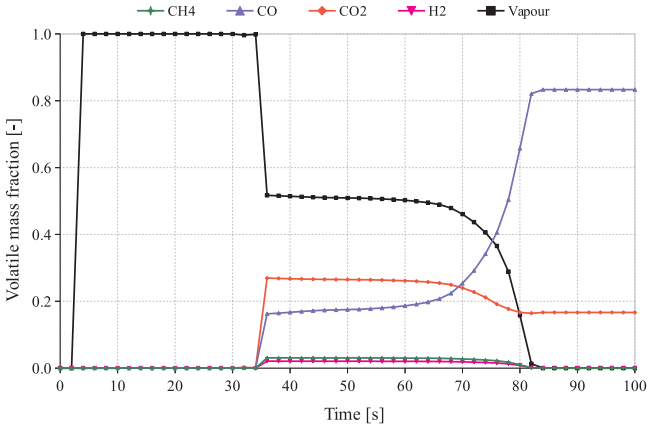

(a) Volatiles mass fraction

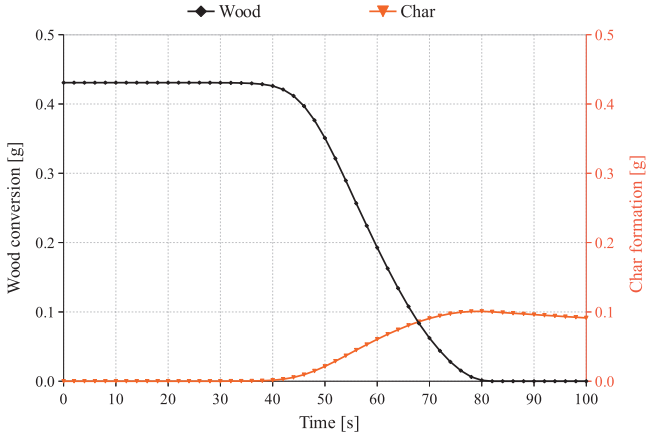

(b) Wood conversion and char formation

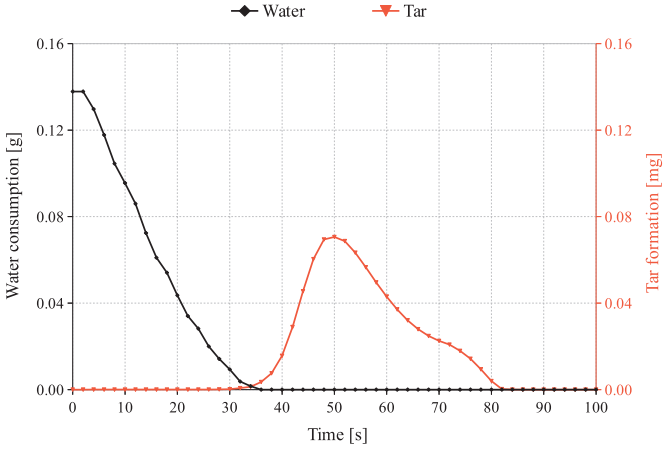

(c) Water consumption and tar formation

Fig. 6. Behavior of gas, solid and liquid products during conversion of cylindrical particle at $T_{wall} = 700\,°C$.

That is the tar product is transferred to the reactor and combusted with oxygen above the particle. This leads to release more carbon monoxide and hydrogen inside the system.

5. Conclusion

In this study, the biomass conversion is investigated with a DEM-CFD coupling approach. This complex platform is developed based on C++ language to take advantage of object oriented programming (OOP). In this approach, the solid particles are considered as discrete elements leading to track the motion of each particle individually based on Newton's equations of motions. In addition, inside of each element (from the surface to core of particle) is discretized radially based on arbitrary number of cells in order to resolve the conservation equations. This leads to evaluating the distribution of temperature and species in any instant. The equations of motions are described based on sphere but due to introducing sub-sphere configurations instead of other types of particles such as slab and cylinder, it is feasible to extend the model for other shapes as well. To resolve the conservation equations in continuous gas phase, OpenFOAM as computational fluid dynamics (CFD) tool (with C++ base as well) is employed and coupled to the solid phase via heat, mass and momentum transport. The coupling is implemented via determining interfaces as source terms between solid-gas phases. According to the applied physical and chemical processes in the system, the relevant homogeneous and heterogeneous reactions are performed in both solid and gas phases. Moreover, related empirical correlations are implemented like heat and mass transfer coefficients which are based on Wakao scheme here. To improve the prediction of model, a shrinking model is also developed to evaluate the effect of shrinkage during biomass conversion. The model is based on the rate of wood and char consumption and the results show a remarkable improvement in the predictions by numerical simulation. It is shown that the conversion process is consist of different stages as heat-up, drying, pyrolysis, gasification and combustion which take place sequentially. Therefore, this multi-physics and multi-scale platform is appropriate for various lab-scale and industrial-scale applications including solid-gas phases. This work as evaluating the single pellet conversion is the preliminary effort for the next study which concerns the conversion of cylindrical biomass particles in a bubbling fluidized bed reactor.

Acknowledgements

The authors would like to thank The Luxembourg National Research Fund (FNR) for supporting this research.

References

[1] A.E. Ghaly, K.N. MacDonald, mixing patterns and residence time determination in a bubbling fluidized bed system, Am. J. Eng. Appl. Sci. 5 (2) (2012) 170–183.
[2] A. Tremel, H. Spliethoff, Gasification kinetics during entrained flow gasification Part i; devolatilisation and char deactivation, Fuel 103 (2013) 663–671.
[3] D. Baruah, D. Baruah, Modeling of biomass gasification: a review, Renew. Sustain. Energy Rev. 39 (2014) 806–815.
[4] B. Babu, P.N. Sheth, Modeling and simulation of reduction zone of downdraft biomass gasifier: effect of char reactivity factor, Energy Convers. Manag. 47 (2006) 2602.
[5] A. Melgar, J.F. Perez, H. Laget, A. Horillo, Thermochemical equilibrium modelling of a gasifying process, Energy Convers. Manag. 48 (2007) 59–67.
[6] N. Gao, A. Li, Modeling and simulation of combined pyrolysis and reduction zone for a downdraft biomass gasifier, Energy Convers. Manag. 49 (2008) 3483–3490.
[7] E. Azzone, M. Morini, M. Pinelli, Development of an equilibrium model for the simulation of thermochemical gasification and application to agricultural residues, Renew. Energy 46 (2012) 248–254.
[8] D.A. Nield, A. Bejan, Convection in Porous Media, Springer, 2006.
[9] G. Lu, J. Third, C. Mller, Discrete element models for non-spherical particle systems: from theoretical developments to applications, Chem. Eng. Sci. 127 (2015) 425–465.
[10] W. Zhong, A. Yu, X. Liu, Z. Tong, H. Zhang, Dem/cfd-dem modelling of non-spherical particulate systems: theoretical developments and applications, Powder Technol. 302 (2016) 108–152.
[11] A. Dziugys, B. Peters, A new approach to detect the contact of two-dimensional elliptical particles, Int. J. Numer. Anal. Methods Geomech. 45 (2001) 1487–1500.
[12] G. Nolan, P. Kavanagh, Random packing of nonspherical particles, Powder Technol. 84 (1995) 199–205.
[13] K. Samiei, Assessment of Implicit and Explicit Algorithms in Numerical Simulation of Granular Matter (Ph.D. Thesis), University of Luxembourg, 2012.
[14] P.A. Cundall, O.D.L. Strack, A discrete numerical model for granular assemblies, Geotecgnique 29 (1979) 47–65.
[15] H. Xiao, J. Sun, Algorithms in a robust hybrid cfd-dem solver for particle-laden flows, Commun. Comput. Phys. 9 (2011) 297–323.
[16] W. Du, X. Bao, J. Xu, W. Wei, Computational fluid dynamics (cfd) modeling of spouted bed: assessment of drag coefficient correlations, Chem. Eng. Sci. 61 (2006) 1401–1420.
[17] D. Gidaspow, Multiphase Flow and Fluidization; Continuum and Kinetic Theory Descriptions, Academic Press, 1994.
[18] Y.H. Man, R.C. Byeong, A numerical study on the combustion of a single carbon particle entrained in a steady flow, Combust. Flame J. 97 (1994) 1–16.
[19] A.H. Mahmoudi, F. Hoffmann, B. Peters, Application of xdem as a novel approach to predict drying of a packed bed, Int. J. Therm. Sci. 75 (2014) 65–75.
[20] J. Hager, M. Hermansson, R. Wimmerstedt, Modelling steam drying of a single porous ceramic sphere experiments and simulations, Chem. Eng. Sci. 52 (1997) 1253–1264.
[21] B. Peters, A. Diugys, R. Navakas, Simulation of thermal conversion of solid fuel by the discrete particle method, Lith. J. Phys. 51 (2011) 91–105.
[22] B. Peters, Classification of combustion regimes in a packed bed based on the relevant time and length scales, Combust. Flame 116 (1999) 297–301.
[23] B. Peters, Numerical simulation of heterogeneous particle combustion accounting for morphological changes, in: Proceedings of the 27th International Conference on Environmental Systems, Lake Tahoe, USA, SAE-paper 972562, July 1997.
[24] B. Peters, The extended discrete element method (xdem) for multi-physics applications, Sch. J. Eng. Res. 2 (2013) 1–20.
[25] R. Bird, W. Stewart, E. Lightfoot, Transport Phenomena, John Wiley & Sons, 1960.
[26] A. Faghri, Y. Zhang, Transport Phenomena in Multiphase Systems, Elsevier Academic Press, 2010.
[27] C.D. Blasi, 45 Dynamic behaviour of stratified downdraft gasifiers, Chem. Eng. Sci. 55 (2000) 2931–2944.
[28] J. Wiese, F. Wissing, D. Hohner, S. Wirtz, V. Scherer, U. Ley, H.M. Behr, Dem/cfd modeling of the fuel conversion in a pellet stove, Fuel Process. Technol. 152 (2016) 223–239.
[29] R. Johansson, H. Thunman, B. Leckner, Influence of intraparticle gradients in modeling of fixed bed combustion, Combust. Flame 149 (2007) 49–62.
[30] A. Mahmoudi, M. Markovic, B. Peters, G. Brem, An experimental and numerical study of wood combustion in a fixed bed using eulerlagrange approach (xdem), Fuel 150 (2015) 573–582.
[31] P. Basu, Biomass Gasification and Pyrolysis, Academic Press Elsevier, 2010.
[32] D.D. Evans, H.W. Emmons, Combustion of wood charcoal, Fire Saf. J. 1 (1) (1977) 57–66.
[33] C.D. Blasi, C. Branca, Kinetics of primary product formation from wood pyrolysis, Ind. Eng. Chem. Res. 40 (2001) 5547–5556.
[34] G. Groppi, E. Tronconi, P. Forzatti, M. Berg, Mathematical modelling of catalytic combustors fuelled by gasified biomasses, Catal. Today 59 (2000) 151–162.
[35] K.M. Bryden, K.W. Ragland, Numerical modeling of a deep, fixed bed combustor, Energy Fuels 10 (1996) 269–275.
[36] B. Peters, A. DÅiugys, R. Navakas, A shrinking model for combustion/gasification of char based on transport and reaction time scales, Mechanika 18 (2) (2012) 177–185.
[37] N. Wakao, S. Kaguei, Heat and Mass Transfer in Packed Beds, 364 Gordon and Breach Science Publishers, New York, NY, 1982.